RSC Advances

PAPER

View Article Online
View Journal | View Issue

Cite this: *RSC Adv.*, 2020, **10**, 29751

Synthesis and photoluminescence properties of hybrid 1D core–shell structured nanocomposites based on ZnO/polydopamine†

Viktoriia Fedorenko,[ac] Roman Viter,*[ac] Radosław Mrówczyński,[b] Daina Damberga,[a] Emerson Coy[b] and Igor Iatsunskyi*[b]

In the present work, we report on the modelling of processes at the zinc oxide and polydopamine (ZnO/PDA) interface. The PDA layer was deposited onto ZnO nanorods (NRs) *via* chemical bath deposition. The defect concentrations in ZnO before and after PDA deposition were calculated and analysed. The ZnONRs/PDA core–shell nanostructures were studied by transmission electron microscopy (TEM), X-ray diffraction (XRD), Raman and Fourier-transform infrared (FTIR) spectroscopy, photoluminescence (PL) measurements, and diffuse reflectance spectroscopy. The TEM and electron energy loss spectroscopy (EELS) measurements confirmed the conformal coating of PDA, while the PL emission from ZnO and ZnONRs/PDA samples showed a reduction of intensity after the PDA deposition. The decrease of defect concentration participating in PL and quantum efficiency explains the PL reduction. Finally, the observed decrease of activation energies and a shift of the PL peaks are attributed to the formation of an additional local electrical field between the PDA and ZnO nanostructures.

Received 1st June 2020
Accepted 4th August 2020

DOI: 10.1039/d0ra04829a

rsc.li/rsc-advances

1 Introduction

Zinc oxide (ZnO) nanostructures are well known materials with advanced structural and optical properties.[1–4] Due to their high refractive index, wide band gap and room temperature photoluminescence, they have been used in different applications, such as optical coatings, photocatalysis,[5–8] optical sensors and biosensors.[2,9,10] The electronic and optical properties of ZnO can be tuned by forming ZnO-composite nanomaterials.[11–14] Metal nanoparticles that exhibit surface plasmon resonance (Au, Ag, *etc.*) and functional polymeric layers (polyaniline, polypyrrole, *etc.*)[15,16] can be deposited on ZnO by chemical and physical methods.[17,18] ZnO-composite nanomaterials have demonstrated tunable electronic and optical properties.[15,16] Moreover, specific functional groups, for binding of different molecules, have been formed on the surface of ZnO-based nanocomposites, opening a broad range of applications, especially in biosensors.[10,19–21]

The polymerization of functional polymers (polypyrrole, polyaniline, *etc.*) on ZnO surfaces requires special conditions, such as a low pH (2–3).[22,23] However, it often results in the dissolution of ZnO template.[24] Therefore, a possible solution is to use an additional redox agent for triggering polymerization at neutral pH or to deposit polymers, synthesized at higher pH (8–10). Among the polymers of interest, polydopamine (PDA) has a very attractive compound. PDA is a biocompatible material that has been used as a versatile coating and platform for biomedical application, drug delivery system preparation, sensors and biosensors, energy storage and batteries as well as photocatalysis.[25–33] The advantage of PDA is its strong adhesive properties that allows to coat any surface both hydrophilic and hydrophobic. So far, PDA has been used to coat many materials *i.e.* alumina, silicon, magnetite, wood, glass, nanodiamonds and other carbon based materials.[34–38] The crucial attribute allowing to use of the PDA in different applications is its biocompatibility, that has been proved under *in vitro* and *in vivo* conditions.[39–44] Routinely, PDA is obtained by oxidative polymerization of dopamine in TRIS buffer at pH 8.5, which could be very promising for ZnO coating. PDA contains both quinone groups and an open-chain primary amine.[45] The first one can be used to functionalized PDA with different moieties baring amino and thiol groups.[46,47] The presence of primary amino group was confirmed by the diazotransfer reaction on PDA coated magnetic nanoparticles, which led to its further exploitation in organocatalysis.[48,49] Importantly, it is suggested that amino and hydroxyl groups contribute to the adhesive properties of PDA.[50]

Indeed, it has been shown that the combination of PDA with ZnO can lead to enhanced performance in solar cells, optical coatings and antimicrobial materials.[51–53] However, the

[a]*Institute of Atomic Physics and Spectroscopy, University of Latvia, Jelgavas 3, Riga, LV-1004, Latvia. E-mail: roman.viter@lu.lv*

[b]*NanoBioMedical Centre, Adam Mickiewicz University in Poznan, Wszechnicy Piastowskiej str. 3, 61-614 Poznan, Poland. E-mail: igoyat@amu.edu.pl*

[c]*Center for Collective Use of Scientific Equipment, Sumy State University, 31, Sanatornaya St., 40018 Sumy, Ukraine*

† Electronic supplementary information (ESI) available. See DOI: 10.1039/d0ra04829a

mechanism of ZnO/PDA interfaces formation and its impact on optical properties has not been revealed yet. The main challenge regarding modelling of PDA/Semiconductor interfaces is the lack of consensus on the PDA structure. Up to this date, scientists are still debating about the final structure of the polymeric product of PDA, preventing for much needed Density Functional Theory (DFT) or other means for modelling the PDA/semiconductor interaction. Therefore, the use of spectroscopy methods is still the best tool available, in order to bring some understanding to the outstanding properties of PDA.[25,54]

Among the possible spectroscopy methods, photoluminescence (PL) is considered to be a powerful tool for analysis of metal oxide nanostructures.[55] Among those oxides, ZnO have shown two emission bands: ultraviolet (free and bound excitons) and visible (vacancies and interstitials).[56] Reshchikov *et al.* showed a methodology for the estimation of defect concentration in ZnO nanostructures by PL analysis.[57,58] This method is based on the sublinear power dependence of defect PL intensity on the excitation power.[57,58] As result, the defect concentration and quantum efficiency could be evaluated.[57,58] Additionally, the activation energies and exciton binding energies in ZnO nanostructures could be evaluated from the temperature quenching of the PL spectra.[57,58] Likewise, the activation energies and exciton binding energies provide important information on the photoinduced processes in ZnO and, more importantly, the role of bulk and surface contributions. Thus, PL is an ideal method for analysing ZnO/PDA nanocomposites, which can bring further insights on the interfacial phenomena occurring on these structures. Comparison of electronic (FTIR, Raman spectroscopy) and optical properties (PL emission) ZnO and ZnO–PDA nanostructures has never been studied before. Mechanisms of PDA layer forming on metal oxide surface and the role of ZnO defects on PDA structure are not revealed yet. Understanding of the above mentioned physical phenomena are important for further applications of PDA-based composites for sensor and biomedical purposes.

In this paper, we report on the analysis of the ZnO/PDA interface by low-temperature PL spectroscopy. The results allow to determine a correlation between the structural and optical properties of ZnONRs and ZnONRs/PDA nanostructures. Furthermore, the role of the PDA layer on PL emission intensity, defect concentrations and the quantum efficiency in ZnO/PDA nanostructures is analysed and discussed. Finally, the photoluminescence results, combined with Raman spectroscopy and FTIR data allow us to propose a model for forming of ZnO/PDA core–shell nanostructures. The results shown in this study provide a unique insight into the electronic process of the ZnO/PDA interface and shine a new light on the understanding of the interaction of PDA with oxide semiconductor surfaces.

2 Experimental section

2.1. Materials

Zinc acetate dehydrate, hexamethylenetetramine, 2-propanol (IPA), ethanolamine, sodium sulphate, zinc nitrate hexahydrate were obtained from Sigma Aldrich (Riga, Latvia), dopamine hydrochloride 99% (10174833), and tris(hydroxmethyl)aminomethane 99% (A18494) were purchased from Alfa Aesar (Poland), and were used without additional purification. The glass substrates (10 mm × 10 mm) were cleaned by successive sonication with deionized water and isopropyl alcohol for 10 min, with proper drying prior to final use. Oxygen plasma treatment for 15 min was performed in order to eliminate organic traces.

2.2. Fabrication of ZnO nanorods

ZnO nanorods (ZnONRs) were deposited by hydrothermochemical method (Fig. 1) as described in Viter *et al.* works.[16,59] Initial ZnO seed layer has been prepared on glass by drop casting of 20 μL of 1 mg mL^{-1} zinc acetate methanol solution, followed by annealing at 350 °C for 1 hour. The glass substrates with ZnO seed layers were incubated for 4 hours in 50 mM of zinc nitrate and 50 mM of hexamethylenetetramine containing solution in water at 95 °C. A hydrothermal growth of ZnONRs was performed. The samples were washed by deionized water and dried at room temperature.

2.3. Deposition of polydopamine on ZnO nanorods

As deposited glass substrates (size 10 × 10 mm^2) with ZnONRs were immersed into a Tris buffer (10 mM, pH 8.5, 50 mL) with a dopamine concentration of 0.4 mg mL^{-1} at room temperature for deposition time 2 hours. In the next step the samples were removed and rinsed with Milli-Q water and dried with nitrogen (N_2) stream.

2.4. Characterization

Structural properties of the ZnONRs–PDA nanostructures were investigated by XRD (PANAlytical Xpert-PRO diffractometer equipped with a Pixel 3D detector using Ni-filtered Cu Kα radiation 45 kV/40 mA), SEM (Zeiss Evo HD15 SEM from Zeiss Ltd (Jena, Germany)), HR-TEM (JEOL ARM 200F) high-resolution transmission electron microscope (200 kV) with

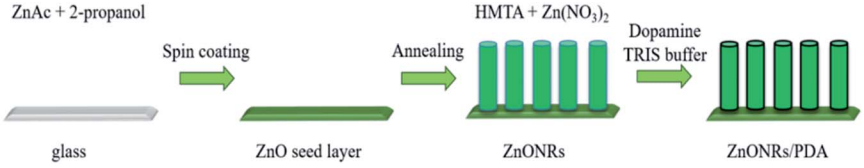

Fig. 1 Schematic diagram of ZnONRs/PDA synthesis by combining hydrothermal method, and dopamine hydrochloride self-polymerization in alkaline aqueous solution.

EDX and EELS detector, Raman scattering measurements were performed using a Renishaw micro-Raman spectrometer equipped with a confocal microscope (Leica) and FTIR spectroscopy, using a FTIR-ATR spectrophotometer 'Frontier' from Perkin Elmer (Waltham, USA). Optical properties were studied by diffuse reflectance spectroscopy, using HR2000+ fiber spectrometer from Ocean Optics (Dunedin, USA). Low-temperature PL properties were studied by homemade setup (see ESI, Fig. S1†). The sample was assembled with copper holder into vacuum chamber with quartz window. Liquid nitrogen was injected into the cavity of the copper holder. The holder was equipped with K-type thermocouple, contacted the surface of the sample. The automatic temperature control was performed with precision of ±1 K. The measurements were performed with a step of 5 K. The PL was excited by Nd:YAG laser (266 nm, output power 29 mW) and collected by spectrometer Horiba iHR320. The measurements were performed in the range of 77–300 K.

3 Results and discussion

The overall process for the synthesis of ZnONRs/PDA is shown in Fig. 1. In the first step glass substrate was covered with ZnONRs by hydro-thermochemical method according to previous report/according to protocol established in our laboratory (precise description is presented at experimental part).[16]

Further obtained glass substrate with ZnONRs was coated with polydopamine using dopamine hydrochloride concentration of 0.4 mg mL^{-1} and time interval 2 hours in order to investigate its influence of optical properties of obtained material. This reaction was performed in Tris buffer at pH 8.5 allowing oxidative polymerization of dopamine.

The structural properties of obtained materials were characterized using X-ray diffraction (see Fig. 2a). In the presented diffractograms peaks located at 31.7°, 34.3°, 36.5°, 47.6°, 56.5°, 62.5° and 68.3° were assigned to (see Fig. 2a) ZnO wurtzite phase.[56] In the XRD spectra of ZnONRs/PDA (see Fig. 2a) no significant changes on crystallinity can be found after the PDA coating, confirming the suitability of PDA for efficient coating of nanosurfaces. Morphology of the synthesized ZnONRs nanostructures was studied by SEM (see Fig. 2b). The diameter of the structures was found to be 50 ± 10 nm, and the length was about 550 ± 50 nm.

The morphology and integrity of the PDA coating on ZnONRs was investigated by TEM (see Fig. 3a and b). These analyses revealed that ZnONRs were uniformly coated with a PDA layer with an average thickness less of ~5 nm. Furthermore, electron energy loss spectroscopy (EELS) analysis on the ZnONRs, proved the presence of nitrogen, carbon, and oxygen, what indicated the formation of PDA in ZnONRs/PDA nanocomposite and confirmed the homogenous coating of ZnONRs. Moreover, since no visible structural changes or degradation of ZnONRs were observed, the deposit condition of PDA required no further optimization.

In order to determine the composition of the produced nanocomposites, Raman spectroscopy was also used.[60] Raman spectra of ZnONRs, PDA and ZnONRs–PDA are shown in Fig. 4a. As prepared ZnONRs showed peaks at 333, 376, and 435 cm^{-1}, related to E_2^{high}–E_2^{low} mode, A_1(TO) polar optical phonon mode, and E_2 (high) non-polar mode, respectively.[61] The observed peak at 435 cm^{-1} (E_2^{high} mode) corresponds to the wurtzite phase of ZnO, as it was also confirmed by XRD. This mode is associated with the vibration of oxygen atoms in the crystal lattice. Raman peak at 586 cm^{-1} could be related to structural disorders (such as oxygen vacancies, Zn interstitial *etc.*).[62] The Raman spectrum of PDA shows two characteristic peaks: 1357 and 1576 cm^{-1}, corresponding to aromatic rings of PDA (stretching and deformation).[63,64]

The ZnONRs–PDA nanostructures showed peaks at 466, 587, 954, 1214, 1386, 1596 cm^{-1}. Raman peaks at 1386 and 1596 cm^{-1} correspond to PDA, and arise from the aromatic C–N stretching mode of the indole structure, and from the C=C aromatic ring vibration, respectively.[65] The results thus confirm the successful deposition of PDA over ZnONRs surface.

Wide peaks at 466 cm^{-1} and 1596 cm^{-1} were deconvoluted in two components *via* Lorentzian fitting. The resulting peaks showed the next values: 457 cm^{-1}, 482 cm^{-1}, 1525 cm^{-1} and 1596 cm^{-1}. The analysis showed good agreement with the

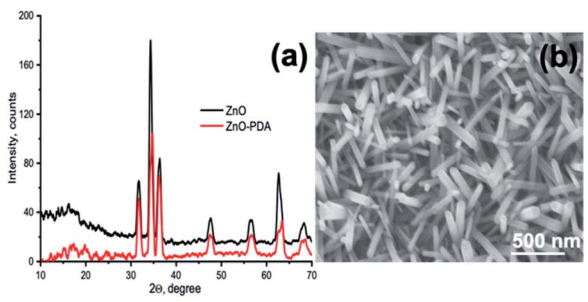

Fig. 2 (a) XRD spectra of ZnONRs and ZnONRs/PDA; (b) SEM image of ZnONRs.

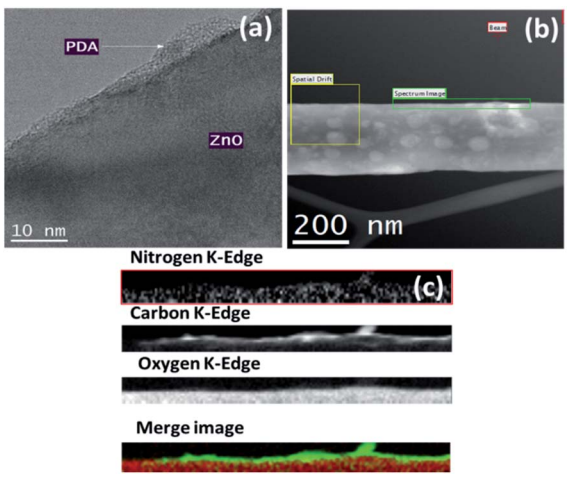

Fig. 3 TEM images of ZnONRs/PDA: (a), and (b); electron energy loss spectroscopy (EELS) analysis of ZnONRs/PDA (c).

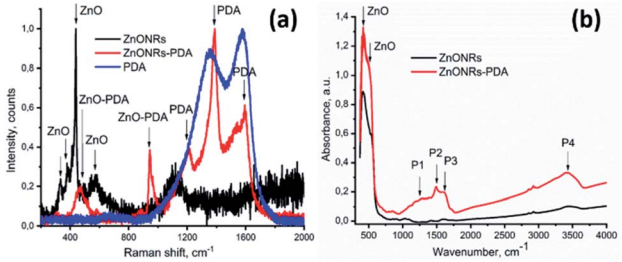

Fig. 4 (a) Raman spectra of ZnONRs, PDA and ZnONRs–PDA; (b) FTIR of ZnO and ZnO–PDA nanocomposites.

present peaks – 1206 cm^{-1}, 1528 cm^{-1} and 1595 cm^{-1}, and 1386 cm^{-1} with the PDA Raman modes, which related to C–OH or/and C–O, C=C, C–N, N–H and C=O vibrations, respectively.[65] Finally, the peak at 457 cm^{-1} relates to ZnO, whereas peaks at 482 cm^{-1} and 954 cm^{-1} correspond to Zn–OH and O–H out-of-plane deformation mode.

FTIR spectroscopy was used to identify of functional groups present on synthesized materials (see Fig. 4b). The peak at 400 cm^{-1} and 560 cm^{-1} was attributed to ZnO vibrational modes. The peaks located at 1288 cm^{-1}, 1492 cm^{-1}, 1607 cm^{-1}, and 3362 cm^{-1} corresponded to C–O, C=N or/and C=C, C=O and –OH or/and N–H vibrational modes, respectively, these modes are in agreement with previously date for PDA.[66] It is important to mention that the formation of PDA layer around ZnO leads to shift the FTIR peak positions of 12–20 cm^{-1} to lower values of wavenumbers.

Optical properties of the ZnO/PDA nanocomposites are not studied well. Due to conformal coating of the PDA over ZnONRs, changes in excitonic and defect emission of ZnONR photoluminescence are expected. We assume that ZnO–PDA interaction might involve ZnO defects. Defect concentration and their type affect optical and electronic properties of ZnO. Therefore, comparison of defect and excitonic parameters in ZnONR and ZnONR–PDA composites will clarify mechanisms of forming the composites. Thus, analysis of PL properties of ZnONRs and ZnONRs/PDA has been performed.

As already mentioned, PL is a simple method for surface defects characterization.[2,13,67] Moreover, the emission *vs.* excitation power allows to evaluate the defect concentration and the quantum efficiency.[2,13,68] The room temperature PL spectra of ZnONRs–PDA showed decrease of intensity and peak shift of ZnO after deposition of PDA layer (see Fig. 5a). We assume two possible mechanisms of the change in ZnONR–PDA PL spectrum: optical absorption by PDA layer and change of emission parameters of ZnO PL (decrease of emission centres concentration, increase of depletion layer, *etc.*).

It was shown correlation between deposition time and PDA layer thickness.[69] Deposition time of 24 hours produced PDA layers with thickness of 70–100 nm. One our deposition of PDA increased layer increase optical density approximately to 0.02 for the whole spectra in the range of 300–800 nm.[69] No characteristic peaks were found. Based on calculation of the thickness of PDA layer and optical absorption we can assume about 6–7% of light absorption by PDA layer in ZnO NR–PDA

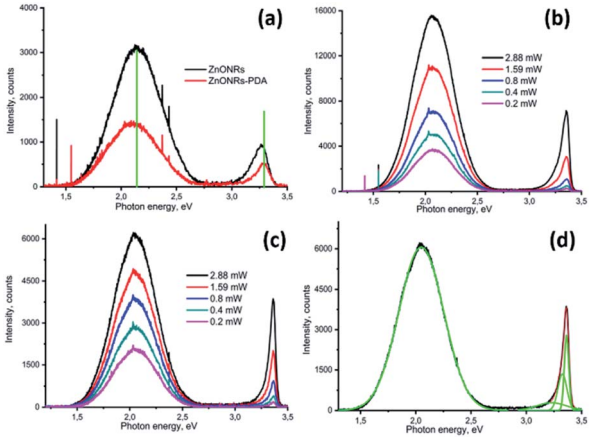

Fig. 5 PL spectra of ZnONRs and ZnONRs–PDA at room temperature (a); ZnONRs (b) and ZnONRs–PDA (c) at 77 K, power dependence; deconvolution of the PL spectrum of ZnONRs–PDA (d).

nanostructure. This optical absorption doesn't explain drastic decrease of ZnONR–PDA PL emission and peak shift. Therefore, a reduction of PL intensity after the PDA deposition could be explained due to the decrease of defect concentration and change of depletion layer on the interface ZnO–PDA. In order to analyse these mechanisms, low temperature measurements of PL of ZnONR and ZnONR–PDA were analysed.

Influence of excitation laser power on PL emission of ZnONRs and ZnONRs–PDA nanostructures was investigated at 77 K (see Fig. 5b and c). Different excitation laser powers were achieved by using neutral filters. The decrease of excitation power resulted in decrease of the PL intensity (Fig. 5b and c). UV emission intensity decreased more drastically, compared to the visible emission. It points to different nature of emission mechanisms.[67]

Previously, we have shown analysis of the ZnO PL spectra and calculations of emission parameters (quantum efficiency and defect concentration).[67] Due to complex behaviour of ZnO emission deconvolution of the emission spectra on separate emission peaks by using Gaussian function is required.[67] The deconvolution of the PL spectrum of ZnO–PDA (Fig. 5 d) showed peaks, located at 2.05, 3.27, 3.348, 3.368 eV. The peaks, located at 3.27–3.368 eV and 2.05 eV were related to exciton and defect emission, respectively.[70] It was found that excitation power dependence of the integrated intensity at 77 K showed sublinear dependence for peaks in the visible range and a superliner dependence for the UV peaks (see Table S1, ESI†). It is known that defects in ZnO are the source of charge carriers, charge traps and emission centres (centres of PL).[67,71,72]

To simplify calculations, we assume that only one emission centre is presented in the forbidden zone of ZnO and the absence of electron and hole traps (Fig. 6a). In this case, the dynamic equation of trapped and free electron concentrations will be described by the following kinetic equations:[73]

$$\frac{dn_t}{dt} = n \times (N_d - n_t) \times C_n - n_t \times C_p \times p \quad (1)$$

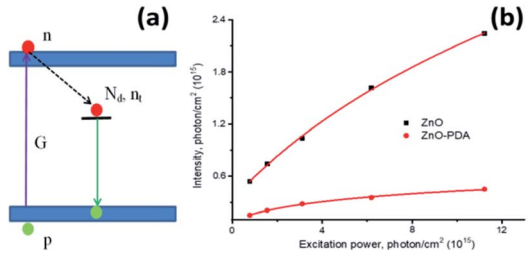

Fig. 6 Diagram of possible radiative and nonradiative transitions (a). The power dependences of integrated intensities for ZnO and ZnO–PDA (b).

$$\frac{dn}{dt} = G - n \times (N_d - n_t) \times C_n - \frac{n}{t} \quad (2)$$

where G – excitation power, n_t – electron concentration in defect levels, N_d-defect concentration, n – free electron concentration, p-free hole concentration, $C_{n,p}$ –electron and hole capture coefficients.

Solving the eqn (1) and (2), the following expression for the emission intensity will be obtained:[73]

$$I = \frac{N_d}{\alpha \times \tau_r} \ln\left(1 + \frac{N_d \times \eta}{\alpha \times \tau_r} \times P\right) \quad (3)$$

where α – absorption coefficient, parameter τ_r characterizes the recombination lifetime, P – average laser excitation power, and η – quantum efficiency.

The power dependences of integrated intensities for ZnONRs and ZnONRs–PDA, replotted in photon per cm^2 are shown in Fig. 6b. The fitting of the curves gave following values for the defect concentration and quantum efficiency: 1.5×10^{15} cm^{-3} and 0.28 and 1.2×10^{14} cm^{-3} and 0.12 for ZnONRs and ZnONRs–PDA, respectively.

Low-temperature PL provides valuable information on the quenching of the emission mechanism of the system. Temperature dependence of PL for ZnONRs and ZnONRs–PDA in the temperature range 77–300 K are presented in Fig. 7a and b. Two effects were observed in both ZnONR and ZnONR–PDA nanostructures: temperature quenching of the PL and shift of the peaks. The increase of the temperature resulted in red shift of PL peak in UV region and blue shift of the visible emission. The effects of the peak shift have been previously discussed.[58,67,74–76] Change of UV peak position is related to temperature dependence of ZnO band gap and transitions between bound and free excitons.[67] Temperature range of this paper (77–300 K) is too high for existence of the bound excitons. As the ZnO band gap continuously decreases with temperature the shift of exciton emission towards lower values is followed.[67]

The increase of the temperature increases the lattice vibrations.[67,75,76] In a number of reports the blue shift of visible emission was explained by electron-phonon coupling.[67,75,76] The phonon coupling resulted in increase of the emitted photon energy.

Temperature quenching of photoluminescence provides information about activation energies and exciton binding energies.[67] The following equation was used for the evaluation of ZnO and ZnO/PDA activation energy of PL quenching:[74]

$$I \sim \frac{1}{1 + A \times \exp^{-\left(\frac{E_a}{k_B T}\right)}} \quad (4)$$

where E_a, k_B and T are activation energy, Boltzmann constant and temperature, respectively. The obtained dependences $I(T)$ were plotted in as $1/I$ *versus* $1/T$ and fitted by an exponential function (Fig. 8a and b) to calculate activation energies. The calculated values are shown in the Table 1. The activation energies obtained for UV peaks correspond to free excitons (0.056 eV) and defect-bound excitons (0.024 and 0.018 eV) in ZnO. It is clearly seen that forming of a PDA layer over the ZnONRs resulted in the decrease of the activation energies, which could be due to the formation of the additional local electrical field between ZnO and PDA layer.

Following model of forming ZnO/PDA interface is proposed. The model scheme of ZnO/PDA nanostructure is represented in Fig. 8c. Based on FTIR and Raman analysis, we assume that PDA is attached to the ZnO *via* –OH groups in PDA structure. Based on PL analysis, the intensity of the peaks and the defect concentration decreased after deposition of PDA over ZnONRs.

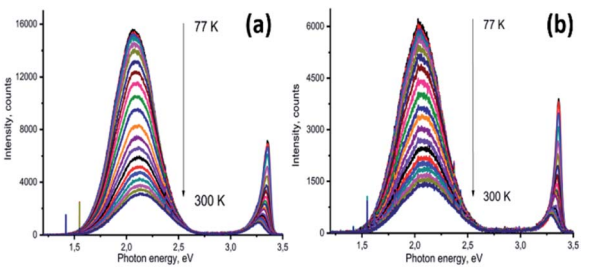

Fig. 7 Photoluminescence temperature dependence of ZnONRs (a) and ZnONRs–PDA (b).

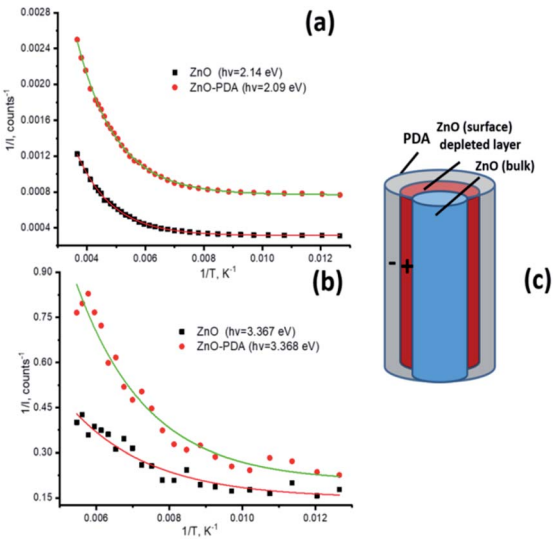

Fig. 8 Exponential approximation for activation energy calculations (a and b). The model of forming ZnO/PDA interface (c).

Table 1 Evaluation of ZnO and ZnO–PDA activation energies

	2.14–2.09 eV	3.28–3.27 eV	3.34–3.33 eV	3.367 eV
ZnO	0.074	0.018	0.024	0.053
ZnO–PDA	0.064	0.01	0.013	0.044

Forming of ZnO/PDA interface involves ZnO defects, particularly doubly ionized oxygen vacancies/or oxygen interstitials. It is assumed that forming of ZnO/PDA interface decrease the concentration of ZnO defects. Due to new surface states, the local electrical field is formed increasing the depletion layer of ZnO. Forming of the additional local field results in a decrease of activation energies and shift of the PL peaks. Previously, it was shown that PL intensity is modulated by the value of the depleted layer in ZnO.[71] Taking into account that the value of depleted layer is proportional to the Debye length, we assume that changes of the Debye length will affect the PL intensity. The Debye length can be estimated as:[71]

$$L_{\mathrm{D}} = \sqrt{\frac{k \times T \times \varepsilon \times \varepsilon_0}{N_{\mathrm{d}} \times q}} \quad (5)$$

where k, T, ε and ε_0 are the Boltzmann's constant, absolute temperature, a dielectric permittivity of ZnO ($\varepsilon = 8.5$) and the electric constant ($\varepsilon_0 = 8.85 \times 10^{-12}$ F m^{-1}), respectively. The full donor or charge carrier concentration in ZnO was taken from the literature and was equal to 1×10^{16} cm^{-3}.[77–79] As for ZnO/PDA, the estimated density of emission centres, which are associated with donor defects, is approximately 0.87×10^{16} cm^{-3}. The calculated value of the Debye length difference between ZnO and ZnO–PDA is about 1.2 nm. The increase of Debye length induces expansion of the depleted layer into the bulk section of the sample and as result, PL quenching and changing of peak position.

The proposed mechanism of PL quenching, proposed for ZnONR–PDA nanostructures here could be spread to other materials and composites where the depleted layer modulation is presented. Taking into account that the depleted layer may be changed under different external factors (*e.g.* adsorption of molecules; external coverage; heterojunction formation; material irradiation *etc.*), the proposed mechanism could also explained the principal of operation of (bio)sensors and detectors.

4 Conclusions

In summary, we have represented a comprehensive modelling of the processes on ZnO/PDA interface. The defect concentrations in ZnO before and after PDA deposition were calculated and analysed and decrease of concentration of defects, participating in PL and quantum efficiency was shown. The correlation between structural and optical properties of ZnO/PDA nanostructures was evaluated. TEM results demonstrated the ability to produce conformal PDA coating over ZnO nanorods. Change of FTIR and Raman spectra, due to the formation of ZnO/PDA composite suggest that PDA is attached to the ZnO *via* –OH groups in PDA structure. Defect levels of ZnO (oxygen vacancies) are involved in forming ZnO–PDA interface. Interaction of the defect levels with hydroxyl groups causes a decrease of the defect concentration, PL intensity and quantum efficiency. A decrease of activation energies and shift of the PL peaks observed in ZnONR–PDA nanostructures is explained by formation of additional electrical local field between PDA and ZnO.

Our studies show the applicability of PDA coatings for controlling and improving semiconductor surfaces. Moreover, the results here presented provide further insights on the electronic response of PDA/Semiconductor materials toward their many optical and electronic applications in sensors and catalysis.

Conflicts of interest

There are no conflicts to declare.

Acknowledgements

V. F. would like to thank the financial support from the project 'Investigation of photoinduced processes in one dimensional ZnO/polydopamine nanostructures', within Latvian Post-doc program (1.1.1.2/VIAA/2/18/279). R. M is grateful for the he financial support of National Science Centre of Poland under research grant OPUS number UMO-2018/31/B/ST8/02460. R. V. acknowledges the financial support from the project '1D ZnO/Polidopamīna kodola čaulas nanostruktūru izstrāde ar uzlabotu jutību un uzlabotām struktūras, elektroniskajām un optiskajām īpašībām', within Latvian LZP fund (Reg. N. LZP 2018/1-0394).

References

1 A. Tamashevski, Y. Harmaza, R. Viter, D. Jevdokimovs, R. Poplausks, E. Slobozhanina, L. Mikoliunaite, D. Erts, A. Ramanaviciene and A. Ramanavicius, *Talanta*, 2019, **200**, 378–386.
2 R. Viter, M. Savchuk, N. Starodub, Z. Balevicius, S. Tumenas, A. Ramanaviciene, D. Jevdokimovs, D. Erts, I. Iatsunskyi and A. Ramanavicius, *Sens. Actuators, B*, 2019, **285**, 601–606.
3 O. Graniel, V. Fedorenko, R. Viter, I. Iatsunskyi, G. Nowaczyk, M. Weber, K. Załęski, S. Jurga, V. Smyntyna and P. Miele, *J. Mater. Sci. Eng. B*, 2018, **236**, 139–146.
4 J. Theerthagiri, S. Sunitha, R. Senthil, P. Nithyadharseni, A. Madankumar, P. Arunachalam, T. Maiyalagan and H.-S. Kim, *Nanotechnology*, 2019, **30**, 27.
5 M. T. Man, J.-H. Kim, M. S. Jeong, A.-T. T. Do and H. S. Lee, *J. Lumin.*, 2017, **185**, 17–22.
6 C. B. Ong, L. Y. Ng and A. W. Mohammad, *Renewable Sustainable Energy Rev.*, 2018, **81**, 536–551.
7 A. Ramirez-Canon, M. Medina-Llamas, M. Vezzoli and D. Mattia, *Phys. Chem. Chem. Phys.*, 2018, **20**, 6648–6656.
8 C. M. Taylor, A. Ramirez-Canon, J. Wenk and D. Mattia, *J. Hazard. Mater.*, 2019, 120799.

9 A. Tamashevski, Y. Harmaza, R. Viter, L. Dubovskaya, E. Slobozhanina, I. Volotovski and A. Ubelis, *Research of zinc oxide nanorods application as a platform for immune biosensors development*, 2016.
10 A. Tereshchenko, M. Bechelany, R. Viter, V. Khranovskyy, V. Smyntyna, N. Starodub and R. Yakimova, *Sens. Actuators, B*, 2016, **229**, 664–677.
11 O. Lupan, V. Postica, R. Adelung, F. Labat, I. Ciofini, U. Schürmann, L. Kienle, L. Chow, B. Viana and T. Pauporté, *Phys. Status Solidi RRL*, 2018, **12**, 1700321.
12 R. A. Gonçalves, A. L. d. O. F. Rossetto, D. J. Nogueira, D. S. Vicentini and W. G. Matias, *Aquat. Toxicol.*, 2018, **197**, 32–40.
13 R. Viter, M. Savchuk, I. Iatsunskyi, Z. Pietralik, N. Starodub, N. Shpyrka, A. Ramanaviciene and A. Ramanavicius, *Biosens. Bioelectron.*, 2018, **99**, 237–243.
14 V. Myndrul and I. Iatsunskyi, *Materials*, 2019, **12**, 2880.
15 M. Turemis, D. Zappi, M. T. Giardi, G. Basile, A. Ramanaviciene, A. Kapralovs, A. Ramanavicius and R. Viter, *Talanta*, 2020, **211**, 120658.
16 R. Viter, K. Kunene, P. Genys, D. Jevdokimovs, D. Erts, A. Sutka, K. Bisetty, A. Viksna, A. Ramanaviciene and A. Ramanavicius, *Macromol. Chem. Phys.*, 2020, **221**, 1900232.
17 L. Su and N. Qin, *Ceram. Int.*, 2015, **41**, 2673–2679.
18 D. Ponnamma, J.-J. Cabibihan, M. Rajan, S. S. Pethaiah, K. Deshmukh, J. P. Gogoi, S. K. Pasha, M. B. Ahamed, J. Krishnegowda and B. Chandrashekar, *Mater. Sci. Eng. C*, 2019, **98**, 1210–1240.
19 Z. Hatami, E. Ragheb, F. Jalali, M. A. Tabrizi and M. Shamsipur, *Bioelectrochemistry*, 2020, **133**, 107458.
20 N. Muthuchamy, R. Atchudan, T. N. J. I. Edison, S. Perumal and Y. R. Lee, *J. Electroanal. Chem.*, 2018, **816**, 195–204.
21 T. Liu, Q. Zhao, Y. Xie, D. Jiang, Z. Chu and W. Jin, *Biosens. Bioelectron.*, 2020, **156**, 112145.
22 S. G. Dhole, S. A. Dake, T. A. Prajapati and S. N. Helambe, *Procedia Manuf.*, 2018, **20**, 127–134.
23 M. Chougule, G. Khuspe, S. Sen and V. Patil, *Appl. Nanosci.*, 2013, **3**, 423–429.
24 J. Han, W. Qiu and W. Gao, *J. Hazard. Mater.*, 2010, **178**, 115–122.
25 J. H. Ryu, P. B. Messersmith and H. Lee, *ACS Appl. Mater. Interfaces*, 2018, **10**, 7523–7540.
26 V. Ball, *Front. Bioeng. Biotechnol.*, 2018, **6**, 109.
27 R. Mrówczyński, *ACS Appl. Mater. Interfaces*, 2017, **10**, 7541–7561.
28 K. Qu, Y. Wang, A. Vasileff, Y. Jiao, H. Chen and Y. Zheng, *J. Mater. Chem. A*, 2018, **6**, 21827–21846.
29 R. Pan, Z. Wang, R. Sun, J. Lindh, K. Edström, M. Strømme and L. Nyholm, *J. Materiomics*, 2019, **5**, 204–213.
30 Z. Wang, J. Li, F. Tang, J. Lin and Z. Jin, *RSC Adv.*, 2017, **7**, 23535–23542.
31 W.-X. Mao, X.-J. Lin, W. Zhang, Z.-X. Chi, R.-W. Lyu, A.-M. Cao and L.-J. Wan, *Chem. Commun.*, 2016, **52**, 7122–7125.
32 A. Sukeri, A. Arjunan and M. Bertotti, *Electrochem. Commun.*, 2020, **110**, 106622.
33 Y. Wang, Y. Jia, Y. Zhou, Y. Wang, G. Zheng, K. Dai, C. Liu and C. Shen, *J. Mater. Chem. C*, 2018, **6**, 8160–8170.
34 Z. Wang, M. Yang, Y. Cheng, J. Liu, B. Xiao, S. Chen, J. Huang, Q. Xie, G. Wu and H. Wu, *Composites, Part A*, 2019, **118**, 302–311.
35 R. Wang, D. Feng, T. Chen, S. Chen and Y. Liu, *J. Alloys Compd.*, 2020, **825**, 154081.
36 G. Liu, Z. Lu, X. Zhu, X. Du, J. Hu, S. Chang, X. Li and Y. Liu, *Sci. Rep.*, 2019, **9**, 1–10.
37 H.-p. Zhang, W. Han, J. Tavakoli, Y.-p. Zhang, X. Lin, X. Lu, Y. Ma and Y. Tang, *Composites, Part A*, 2019, **116**, 62–71.
38 J. C. Zuaznabar-Gardona and A. Fragoso, *Sens. Actuators, B*, 2018, **273**, 664–671.
39 H. Lee, S. M. Dellatore, W. M. Miller and P. B. Messersmith, *Science*, 2007, **318**, 426–430.
40 J. H. Cho, V. Vasagar, K. Shanmuganathan, A. R. Jones, S. Nazarenko and C. J. Ellison, *Chem. Mater.*, 2015, **27**, 6784–6790.
41 M. Martín, P. Salazar, R. Villalonga, S. Campuzano, J. M. Pingarrón and J. L. González-Mora, *J. Mater. Chem. B*, 2014, **2**, 739–746.
42 D. Maziukiewicz, B. F. Grześkowiak, E. Coy, S. Jurga and R. Mrówczyński, *Biomimetics*, 2019, **4**, 3.
43 A. Woźniak, M. Walawender, D. Tempka, E. Coy, K. Załęski, B. F. Grześkowiak and R. Mrówczyński, *Toxicol. in Vitro*, 2017, **44**, 256–265.
44 X. Liu, J. Cao, H. Li, J. Li, Q. Jin, K. Ren and J. Ji, *ACS Nano*, 2013, **7**, 9384–9395.
45 J. r. Liebscher, R. Mrówczyński, H. A. Scheidt, C. Filip, N. D. Hădade, R. Turcu, A. Bende and S. Beck, *Langmuir*, 2013, **29**, 10539–10548.
46 J. Liebscher, *Eur. J. Org. Chem.*, 2019, **2019**, 4976–4994.
47 R. Mrówczyński, R. Markiewicz and J. Liebscher, *Polym. Int.*, 2016, **65**, 1288–1299.
48 R. Mrówczyński, A. Bunge and J. Liebscher, *Chem.–Eur. J.*, 2014, **20**, 8647–8653.
49 R. Mrówczyński, L. Magerusan, R. Turcu and J. Liebscher, *Polym. Chem.*, 2014, **5**, 6593–6599.
50 P. Kord Forooshani and B. P. Lee, *J. Polym. Sci., Part A: Polym. Chem.*, 2017, **55**, 9–33.
51 N. Ahmad, X. Zhang, S. Yang, D. Zhang, J. Wang, S. uz Zafar, Y. Li, Y. Zhang, S. Hussain and Z. Cheng, *J. Mater. Chem. C*, 2019, **7**, 10795–10801.
52 L. Ai, Y. Wang, G. Tao, P. Zhao, A. Umar, P. Wang and H. He, *Molecules*, 2019, **24**, 503.
53 Y. Yang and W. Hu, *Talanta*, 2017, **166**, 141–147.
54 M. Cîrcu and C. Filip, *Polym. Chem.*, 2018, **9**, 3379–3387.
55 R. Viter, K. Jekabsons, Z. Kalnina, N. Poletaev, S. Hsu and U. Riekstina, *Nanotechnology*, 2016, **27**, 465101.
56 R. Viter, A. A. Chaaya, I. Iatsunskyi, G. Nowaczyk, K. Kovalevskis, D. Erts, P. Miele, V. Smyntyna and M. Bechelany, *Nanotechnology*, 2015, **26**, 105501.
57 M. Reshchikov, A. Usikov, H. Helava, Y. Makarov, V. Prozheeva, I. Makkonen, F. Tuomisto, J. Leach and K. Udwary, *Sci. Rep.*, 2017, **7**, 9297.

58 M. A. Reshchikov, A. A. Kvasov, M. F. Bishop, T. McMullen, A. Usikov, V. Soukhoveev and V. A. Dmitriev, *Phys. Rev. B: Condens. Matter Mater. Phys.*, 2011, **84**, 075212.
59 A. Tamashevski, Y. Harmaza, E. Slobozhanina, R. Viter and I. Iatsunskyi, *Molecules*, 2020, **25**, 3168.
60 I. Iatsunskyi, G. Nowaczyk, S. Jurga, V. Fedorenko, M. Pavlenko and V. Smyntyna, *Optik*, 2015, **126**, 1650–1655.
61 I. Mihailova, V. Gerbreders, E. Tamanis, E. Sledevskis, R. Viter and P. Sarajevs, *J. Non-Cryst. Solids*, 2013, **377**, 212–216.
62 R. Viter, V. Khranovskyy, N. Starodub, Y. Ogorodniichuk, S. Gevelyuk, Z. Gertnere, N. Poletaev, R. Yakimova, D. Erts and V. Smyntyna, *IEEE Sens. J.*, 2014, **14**, 2028–2034.
63 G. Yeroslavsky, R. Lavi, A. Alishaev and S. Rahimipour, *Langmuir*, 2016, **32**, 5201–5212.
64 X. Yu, H. Fan, Y. Liu, Z. Shi and Z. Jin, *Langmuir*, 2014, **30**, 5497–5505.
65 D. Chen, Y. Mei, W. Hu and C. M. Li, *Talanta*, 2018, **182**, 470–475.
66 H. Luo, C. Gu, W. Zheng, F. Dai, X. Wang and Z. Zheng, *RSC Adv.*, 2015, **5**, 13470–13477.
67 D. Damberga, R. Viter, V. Fedorenko, I. Iatsunskyi, E. Coy, O. Graniel, S. b. Balme, P. Miele and M. Bechelany, *J. Phys. Chem. C*, 2020, **124**, 9434–9441.
68 R. Viter, A. Tereshchenko, V. Smyntyna, J. Ogorodniichuk, N. Starodub, R. Yakimova, V. Khranovskyy and A. Ramanavicius, *Sens. Actuators, B*, 2017, **252**, 95–102.
69 M. L. Alfieri, L. Panzella, S. L. Oscurato, M. Salvatore, R. Avolio, M. E. Errico, P. Maddalena, A. Napolitano and M. d'Ischia, *Biomimetics*, 2018, **3**, 26.
70 A. Janotti and C. G. Van de Walle, *Phys. Rev. B: Condens. Matter Mater. Phys.*, 2007, **76**, 165202.
71 R. Viter, I. Iatsunskyi, V. Fedorenko, S. Tumenas, Z. Balevicius, A. Ramanavicius, S. Balme, M. Kempiński, G. Nowaczyk and S. Jurga, *J. Phys. Chem. C*, 2016, **120**, 5124–5132.
72 M. A. Reshchikov, X. Gu, B. Nemeth, J. Nause and H. Morkoç, *MRS Online Proc. Libr.*, 2005, 892.
73 M. Reshchikov and R. Korotkov, *Phys. Rev. B: Condens. Matter Mater. Phys.*, 2001, **64**, 115205.
74 M. A. Reshchikov and H. Morkoç, *J. Appl. Phys.*, 2005, **97**, 5–19.
75 M. Reshchikov, J. Xie, B. Hertog and A. Osinsky, *J. Appl. Phys.*, 2008, **103**, 103514.
76 M. Reshchikov, H. Morkoc, B. Nemeth, J. Nause, J. Xie, B. Hertog and A. Osinsky, *Phys. B*, 2007, **401**, 358–361.
77 W. Lin, D. Chen, J. Zhang, Z. Lin, J. Huang, W. Li, Y. Wang and F. Huang, *Cryst. Growth Des.*, 2009, **9**, 4378–4383.
78 D. C. Look, *Superlattices Microstruct.*, 2007, **42**, 284–289.
79 Z.-Q. Fang, B. Claflin, D. C. Look and G. C. Farlow, *J. Appl. Phys.*, 2007, **101**, 086106.